Study of Low Temperature Deposition of Nanocrystalline Diamond Films on ZnO/LiNbO3 Layered Structures Suitable for Waveguiding Layer Acoustic Wave Devices

Damia Dekkar, Fabien Bénédic, Cécile Floer, Sami Hage-Ali, Ovidiu Brinza, Jocelyn Achard, Omar Elmazria

Study of low temperature deposition of nanocrystalline diamond films on $ZnO/LiNbO_3$ layered structures suitable for Waveguiding Layer Acoustic Wave devices

Damia Dekkar[1], Fabien Bénédic[*,1], Cécile Floer[2], Sami Hage-Ali[2], Ovidiu Brinza[1], Jocelyn Achard[1] and Omar Elmazria[2]

[1] LSPM-CNRS, Université Paris 13, 99 Avenue Jean-Baptiste Clément, 93430 Villetaneuse, France
[2] Institut Jean Lamour-CNRS, Université de Lorraine, 2 allée André Guinier, 54011 Nancy, France

Received ZZZ, revised ZZZ, accepted ZZZ
Published online ZZZ (Dates will be provided by the publisher.)

Keywords NanoCrystalline Diamond, Waveguiding Layer Acoustic Wave, piezoelectric materials, low temperature growth

* Corresponding author: e-mail fabien.benedic@lspm.cnrs.fr, Phone: +33 149403 423, Fax: + 33 149403 414

In this paper the NanoCrystalline Diamond (NCD) film low temperature deposition process on ZnO/Si, $ZnO/LiNbO_3$ and $ZnO/IDTs/LiNbO_3$ substrates is investigated aiming at obtaining layered structures suitable for Waveguiding Layer Acoustic Wave (WLAW) devices. The NCD synthesis is performed at 250 °C by using a Distributed Antenna Array (DAA) microwave system operating in $H_2/CH_4/CO_2$ gas mixture at low pressure (<1 mbar).

Since the ZnO layer is etched during the NCD growth process, the deposition of a thin AlN layer of few hundred nanometers in thickness on the considered substrates is performed and is shown to be effective as a protective layer. Diamond growth on AlN-coated ZnO/Si substrates emphasizes the ability of the DAA reactor to synthesize NCD films with properties similar to those obtained on silicon substrates. Besides adherent NCD films up to 300 nm thickness are synthesized on AlN-coated $ZnO/LiNbO_3$ substrates but stress in the layered structure appears during the plasma process. Finally, the feasibility of a $NCD/AlN/ZnO/IDTs/LiNbO_3$ layered structure, suitable for WLAW devices, is successfully demonstrated, even if the NCD film adherence must be further improved on the Inter-Digital Transducers (IDTs) finger zone.

1 Introduction Diamond is a material of choice for many technological applications, in particular for Surface Acoustic Wave (SAW) and Waveguiding Layer Acoustic Wave (WLAW) structures, because of its exceptional-mechanical, electrical and thermal properties [1]. In particular, with its low surface roughness (≤ 20 nm) and its very high acoustic velocity (≥ 10 $km.s^{-1}$), nanocrystalline diamond (NCD) is worthy of note as an acoustic material for SAW devices [2,3]. However, SAW device packaging, generally costly and bulky, remains a real bottleneck, which can be solved by using the WLAW concept. Thus, the WLAW principle is based on wave confinement in a low acoustic velocity layer enclosed between two high velocity materials. Moreover, one of the layers has to be piezoelectric to allow the generation of the acoustic wave.

Promising results have been obtained by using the $AlN/ZnO/IDTs/LiNbO_3$ multilayered structure for packageless body centric sensors [4]. In this configuration, the Inter-Digital Transducers (IDTs) are deposited on the $LiNbO_3$ substrate; AlN and $LiNbO_3$ have a high acoustic velocity compared to ZnO; and $LiNbO_3$ is characterized by a high electromechanical coupling coefficient and weak acoustic wave propagation losses [5-7]. Recently, it was shown that the use of a sputtered AlN film of 6 µm thickness causes acoustic losses during propagation, while theoretical calculations pointed out that using only 2.5 µm of diamond films would be sufficient to confine the wave and

to reduce the propagation losses [8]. Moreover, the wave confinement should be improved with the diamond layer. Besides, due to its exceptional hardness and chemical inertness, the diamond film would play a key role by protecting the SAW device from environment contaminations. Thus, the NCD/ZnO/IDTs/$LiNbO_3$ structure is a promising layered structure to achieve high performance WLAW devices.

Most of NCD synthesis processes, especially the usual Microwave Plasma Assisted chemical Vapor Deposition (MPACVD) process, generally require substrate temperatures above 400 °C. This high substrate temperature will destroy the transducers and make ZnO and $LiNbO_3$ lose their piezoelectric properties [9]. For these reasons, low temperature synthesis of NCD films is needed in order to overcome these inherent drawbacks.

In this work, we investigate the low temperature synthesis of NCD films on various layered structures by using a distributed antenna array (DAA) system operating in $H_2/CH_4/CO_2$ gas mixture at low pressure (< 1 mbar) [10]. NCD films grown at 250 °C on ZnO/Si and ZnO/$LiNbO_3$ substrates, and finally on the ZnO/IDTs/$LiNbO_3$ layered structure suitable for WLAW devices, are characterized in terms of morphology and microstructure, and solutions are examined in order to preserve the substrate integrity.

2 Experimental

Different substrate configurations were achieved: ZnO/Si, ZnO/$LiNbO_3$ and ZnO/IDTs/$LiNbO_3$. ZnO was deposited using Radio-Frenquecy (RF) magnetron sputtering with the following parameters: 4-inch Zn target, 150 W, $6x10^{-3}$ mbar, 6 sccm O_2 and 6 sccm N_2. Two deposition temperatures of ZnO at 170 °C and 25 °C were tested. The ZnO layers were synthesized on silicon substrates ((100)-oriented, thickness of around 380 µm) or on a $LiNbO_3$ 128° Y-cut substrate (MTI Corporation). Since the thickness of ZnO thin films affects strongly the device performance and the wave confinement [9], a maximum thickness of 2 µm was deposited.

In some case, a thin AlN protective coating (thickness of 150 or 300 nm) was also deposited with non-intentional heating on the ZnO surface using RF magnetron sputtering with the following parameters: 4-inch Al target, 200W, $8x10^{-3}$ mbar and 16 sccm N_2.

Considering the expected NCD-based WLAW devices, a ZnO/IDTs/$LiNbO_3$ layered structure was realized. First 10 nm of titanium (Ti) as adhesion layer and 90 nm of gold (Au) were deposited on a $LiNbO_3$ substrate by RF magnetron sputtering and IDTs(Ti/Au) were fabricated using the electron beam lithography process. A negative resist was used to limit the processing time. Ion Beam Etching (IBE) and O_2-plasma treatment were used to finalize the IDT manufacturing. The synchronous resonator obtained has the following parameters (Figure 1):

- A period of the IDTs λ=4.4µm to reach a 868 MHz central frequency;
- 100 finger pairs for the resonator and 200 fingers for the two reflectors forming the Bragg mirror;
- The metallization ratio is fixed to 60% leading to a resolution of 1.32µm;
- The aperture (length of the fingers) is set at the value of 269µm.

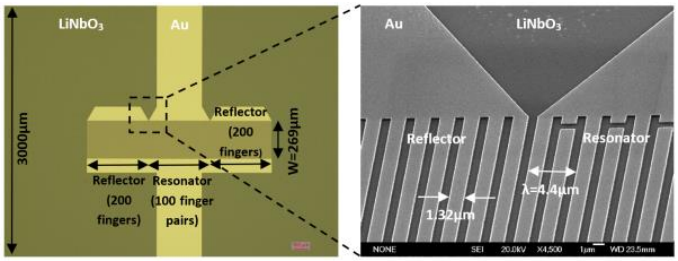

Figure 1 Top view of a microfabricated SAW device formed of IDTs(Ti/Au)/$LiNbO_3$ before ZnO deposition.

NCD film deposition was carried out with a DAA microwave system which consists of 16 plasma sources arranged in 4x4 matrix. Discharge is ignited in a $H_2/CH_4/CO_2$ feed gas. Such configuration, details of which can be found elsewhere [11], showed its efficiency for the NCD growth on 4-inch silicon substrates at low pressure (< 1 mbar) and low temperature (< 400 °C). Note that the addition of CO_2 in the feed gas is required for low temperature synthesis in order to improve the etching of non-diamond phase, as discussed in [11] and reference therein. The main advantage of this reactor is to enable the growth of NCD films on large areas with satisfactory growth rates, while allowing an easy up-scaling and industrial implementation. For the present study, typical NCD growth conditions were employed: a microwave power of 3 kW, a 96.4%/2.6%/1% $H_2/CH_4/CO_2$ gas mixture under 0.35 mbar and 50 sccm flow rate. The substrate temperature, measured with a thermocouple in mechanical contact with the bottom of the substrate holder, was controlled at 250 °C using a PID system. Before growing, the substrates were seeded by spin coating with a colloidal solution containing diamond nanoparticles produced by detonation.

Si reference and ZnO/Si (S1 sample) samples were seeded using a 25 nm grain size powder with highly negative zeta potential (SYP-GAF-0-0.05 provided by Van Moppes). The colloidal solution was diluted in water and, in order to avoid coagulation, PVA (PolyVinyl Alcohol) powder was added.

In order to improve the nucleation density on AlN-coated substrates, samples were specifically seeded by a nanodiamond aqueous solution with a grain size of 4-6 nm and a highly negative zeta potential (VOX d provided by Carbodeon). As a matter of fact, the negative zeta potential of this solution is due to its carboxylate function group surface. When AlN is immersed into the water-based colloidal diamond solution, the surface rapidly hydrolyzes by forming AlOOH and/or Al(OH). This implies the formation of hydroxyl group which forms a positively charged surface [12]. Therefore, the electrostatic attraction occurs between

the diamond particles and the AlN surface, which leads to a high seeding density and consequently to a high nucleation density which is favorable to the NCD growth but also acts as a protective coating for the AlN and ZnO layers. Note that no other pretreatment, such as N_2, O_2 or CF_4 plasma exposure, has been carried out when using AlN-coated substrates.

The NCD deposition time was varied from 3 up to 7 h.

Table 1 summarizes the substrate characteristics and NCD deposition times, the diamond film properties of which being discussed hereafter.

Table 1 Substrate characteristics and NCD deposition times. The properties of these synthesized NCD films, deposited at 250 °C, are investigated and discussed in section 3. Th_{AlN} and Th_{ZnO} are respectively the aluminum nitride (AlN) and zinc oxide (ZnO) deposited thicknesses measured by profilometer and checked by SEM cross-sectional images, and T_{ZnO} is the ZnO deposition temperature.

Sample	Substrate	Th_{AlN} (nm)	Th_{ZnO} (µm)	T_{ZnO} (°C)	NCD deposition time (h)
S1	ZnO/Si	0	0.9	170	4
S2	AlN-coated ZnO/Si	150	1.2	25	6
S3	AlN-coated ZnO/$LiNbO_3$	300	2	25	7
S4	AlN-coated ZnO/IDTs/$LiNbO_3$	300	2	25	3

The film morphology was investigated by top-view Scanning Electron Microscopy (SEM) taken by a field emission ZEISS ULTRA plus SEM system. Surface topography was estimated with a VEECO Dimension 3100 Atomic Force Microscopy (AFM) system in tapping mode in air. The Raman spectra were obtained with a HR800 (HORIBA Jobyn-Yvon) apparatus operating at 458 nm excitation wavelength. It was used to analyze the phase purity of the deposited diamond films and identify the substrate contributions. X-Ray Diffraction (XRD) patterns were obtained using $CuK_{\alpha 1}$ radiation (λ= 1.54056 Å) with an incident X-ray angle of 2° in order to analyze the sample composition and crystalline properties. The NCD film grain size was estimated using a Rietveld method applied on the (111) and/or (220) diffraction peaks [13].

In order to easily estimate the NCD film thickness, the growth was systematically and simultaneously performed both on a Si substrate, as reference, and on the considered substrates (ZnO/Si, ZnO/$LiNbO_3$ or ZnO/IDTs/$LiNbO_3$). Indeed, the growth rate only depends on experimental parameters, regardless of the substrate nature if the deposition temperature is maintained constant [14], so that the resulting film thickness can be considered similar whatever the substrate. NCD film deposited thickness (Th_{NCD}) was then estimated on Si substrate by using a UV-visible reflectometer and by measuring the weight gain after deposition according to equation (1).

$$\mathrm{Th_{NCD}} = \frac{\left(\frac{\mathrm{m_{after}} - \mathrm{m_{Si}}}{\rho_D}\right)}{\frac{\mathrm{m_{Si}}}{\rho_{Si}} \times \frac{1}{\mathrm{Th_{Si}}}} \quad (1)$$

Where m_{Si} and m_{after} are the silicon weight and the weight measured after growth, respectively, ρ_{Si} and ρ_D are the silicon and diamond densities, respectively, and Th_{Si} is the silicon thickness before growth.

Knowing Th_{NCD} determined on Si substrate, the weight variation of ZnO/Si samples before and after growth permits to estimate the ZnO consumption encountered during diamond deposition from equation (2).

$$\mathrm{Th}^{etch}_{\mathrm{ZnO}} = \frac{(\mathrm{m_{before}} - \mathrm{m_{after}})}{\frac{\mathrm{m_{before}}}{\mathrm{Th_{ZnO}}\cdot\rho_{\mathrm{ZnO}} + \mathrm{Th_{Si}}\cdot\rho_{\mathrm{Si}}}\cdot\rho_{\mathrm{ZnO}}} + \mathrm{Th_{NCD}} \cdot \frac{\rho_{\mathrm{NCD}}}{\rho_{\mathrm{ZnO}}} \quad (2)$$

Where Th^{etch}_{ZnO} is the ZnO etched thickness, ρ_{ZnO} is the ZnO density, and m_{before} is the ZnO/Si substrate weight before the NCD growth.

The NCD film thickness was also obtained in real time by using *in situ* Laser Reflectance Interferometry (LRI) on the Si sample, which permits to stop the deposition process when the expected thickness is reached [15].

3 Results and discussion

3.1 NCD deposition on ZnO/Si and AlN-coated ZnO/Si substrates In order to demonstrate the feasibility of NCD growth on ZnO layer, ZnO/Si substrates were first investigated (S1 sample). The synthesis was carried out for 4 h (Table 1) with growth conditions usually employed on Si substrates at 250 °C surface temperature.

The weight gain, as well as reflectometry and LRI measurements, show that the NCD film thickness deposited simultaneously in these conditions on Si reference substrate is around 170 nm. However, the weight gain is negative for the ZnO/Si sample, which indicates that the diamond synthesis did not occur and/or that the ZnO layer was partially or totally etched during the NCD growth. The SEM micrograph presented in Figure 2 exhibits a granular surface typical of NCD films produced in the DAA reactor [16], which proves that, in spite of the weight loss, the diamond growth took place. The film is homogeneous, continuous and covers the entire sample surface, and its surface roughness is about 11 nm, which is comparable to the values already reported on silicon substrate [16].

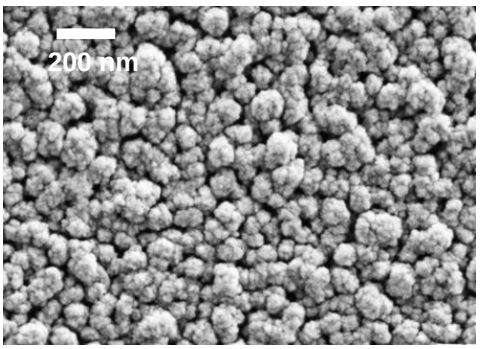

Figure 2 SEM micrograph of NCD film deposited on S1 sample (ZnO/Si).

The Raman spectrum of Figure 3 exhibits the characteristic peak of diamond at 1332 cm^{-1}, which confirms the presence of carbon sp^3 phase on S1 sample. The Full Width at Half Maximum (FWHM) of the diamond peak is around 14 cm^{-1}, which is typical of the nanocrystalline feature. The ZnO contribution, that appears around 1150 cm^{-1} [17] as shown on the Raman spectrum of the ZnO/Si bare substrate, cannot be easily identified after NCD growth. This is consistent with the fact that the ZnO layer is partially or totally consumed during the plasma process.

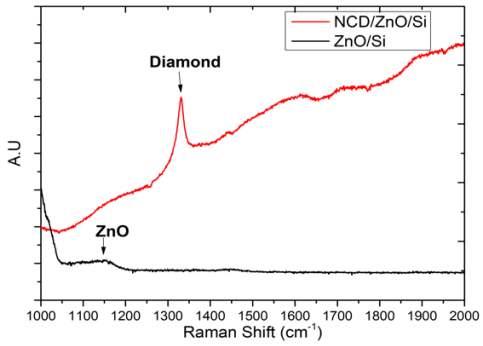

Figure 3 Raman spectra of S1 sample (ZnO/Si) before and after NCD growth.

This hypothesis is confirmed by the XRD diffraction pattern of S1 sample after NCD deposition (Figure 4), where only the diffraction peaks corresponding to diamond and silicon can been clearly observed. Indeed, the three peaks at 2θ = 44.1°, 75.6° and 91.7° are relative to the (111), (220) and (311) crystalline plans of cubic diamond (JCPDS, No.6-0675), respectively, whereas the (311) diffraction peak of silicon appears at 2θ=56.2 ° (JCPDS, No.27-1402). The diamond grain size estimated from the XRD pattern is about 10 nm, which is similar to the value reported for the same growth conditions on silicon substrate [16].

This implies that the ZnO layer is etched by the deposition plasma fed with $H_2/CH_4/CO_2$ gas mixture. As a matter of fact, assuming that the NCD thickness deposited on S1 sample is similar to the one measured on Si reference substrate, the ZnO etched thickness Th^{etch}_{ZnO} was estimated around 500 nm through equation (2), which corresponds to more than the half of the initial ZnO thickness (900 nm). This points out that there is a competition between NCD growth and ZnO etching. It should be also emphasized that the etching rate of ZnO layer, measured in the same conditions but in a H_2 plasma (*i.e.* without carbon containing precursors in the gas phase), is as high as 5 µm.h^{-1}. It means that the 0.9 µm-thick ZnO layer of S1 sample can be completely removed after less than 15 minutes of hydrogen plasma, which shows how ZnO is sensitive to the plasma reactive species. This preliminary study thus demonstrates the feasibility of synthesizing NCD films on ZnO layers, but solutions must be found in order to avoid the ZnO consumption aiming at keeping the required thickness for the expected WLAW structure.

In order to preserve the ZnO samples from the reactive NCD deposition plasma, thin aluminum nitride (AlN) films (150 or 300 nm thickness) were tested as protective coatings. It should be recalled here that AlN was first expected as the top layer for WLAW structures and that the purpose is to replace it by a more efficient diamond layer. It can be thus assumed that the acoustic wave confinement and propagation in the ZnO layer would not be strongly affected by this thin AlN layer, while the wave confinement is supposed to be insured by a sufficiently thick NCD film deposited on AlN. All the substrates considered in the following (ZnO/Si, ZnO/$LiNbO_3$ and ZnO/IDT/$LiNbO_3$) were then coated with AlN and will be denominate "AlN-coated *substrate*". After the NCD deposition the samples will be denominate "NCD/AlN/*substrate*".

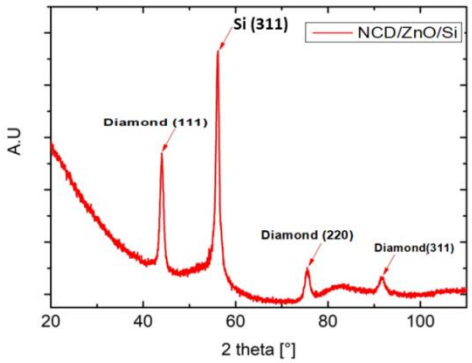

Figure 4 XRD pattern of S1 sample (ZnO/Si) after NCD growth.

Figure 5 presents the SEM micrograph (cross section and top view) of a NCD film deposited on the AlN-coated ZnO/Si substrate corresponding to S2 sample (150 nm AlN, 1.2 µm ZnO, see Table 1). The NCD/AlN/ZnO/Si layered structure obtained after 6 h NCD synthesis is clearly visible with thicknesses of 250 nm, 150 nm and 1.2 µm for the NCD, AlN and ZnO layers, respectively. The initial thickness of AlN and ZnO on S2 sample are thus retrieved. This highlights the efficiency of the AlN coating to prevent the ZnO layer from etching due to the reactive plasma. The morphology of the growing surface is characteristics of NCD films with a granular structure homogeneously covering the entire sample surface. It should be noticed that the diamond particle size is much smaller for S2 sample than for S1 sample. This can result of a difference in the nucleation density on both samples, which could be linked to the ZnO etching in the case of S1 sample. A surface roughness as low as 10 nm is thus reached on S2 sample.

Figure 6 exhibits the Raman spectrum obtained on S2 sample after NCD growth. It is comparable to what is usually obtained on silicon substrates treated in the DAA reactor [16]. The FWHM of the diamond peak observed at 1332 cm^{-1} is slightly narrower than S1 sample with a value of 12 cm^{-1}. The band at 1150 cm^{-1} could be assigned to trans-polyacetylene [18] but is more probably due to the contribution of the ZnO substrate as observed on the AlN-coated ZnO/Si substrate before growth (Figure 6). This is consistent with the SEM micrographs of Figure 5 showing that the ZnO layer is still present in the sample with its initial thickness of 1.2 µm. It should be noted that no AlN contribution is identified before or after NCD growth on the considered Raman spectra, whereas the XRD patterns

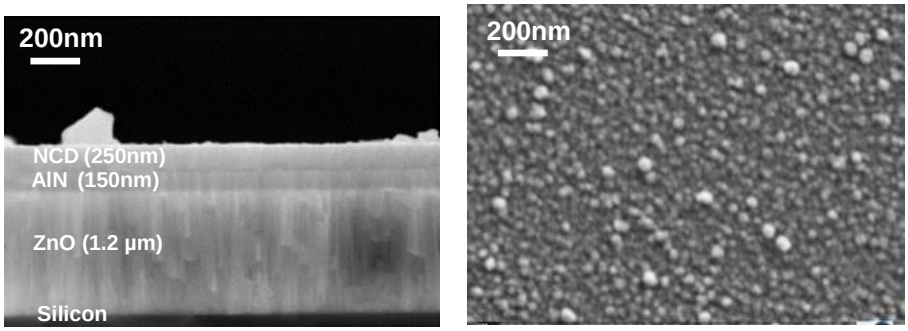

Figure 5 SEM micrographs (cross section and top view) of a NCD/AlN/ZnO/Si sample after NCD growth (S2 sample).

shown in Figure 7 highlights the presence of a crystalline AlN layer.

Indeed, different diffraction peaks corresponding to AlN, ZnO and Si are clearly observed on the XRD spectra of S2 sample before and after NCD growth. The most important contribution is due to the (103) diffraction peak of ZnO film at 2θ = 62.4 ° (JCPDS, No.36-1451) [19], which is slightly shifted after NCD growth. The three peaks at 2θ = 34.2 °, 35.8 ° and 65.7° are relative to the (100), (002) and (103) crystalline plans of hexagonal AlN (JCPDS, No.25-1133**)**. The other two peaks observed at 2θ = 43.6 ° and 74.8 ° after growth are relative to the (111) and (220) crystalline plans of cubic diamond, respectively. The NCD grain size is estimated at 13 nm, which is close to the value reported for S1 sample. The XRD patterns definitely confirm that the ZnO layer is successfully preserved owing to the protective coating of AlN.

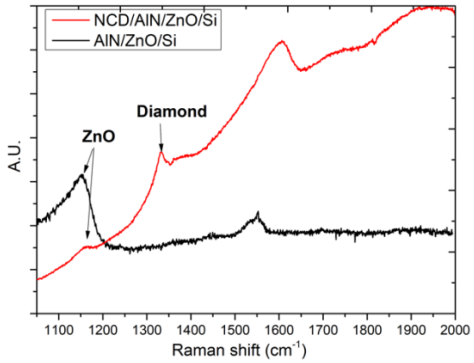

Figure 6 Raman spectra of S2 sample (AlN-coated ZnO/Si) before and after NCD growth.

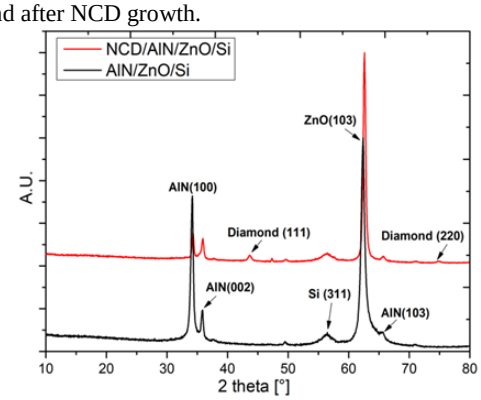

Figure 7 XRD patterns of S2 sample (AlN-coated ZnO/Si) before and after NCD growth.

In this part, the effectiveness of the AlN coating for protecting the ZnO layer from plasma etching was demonstrated for the ZnO/Si layered structure. In the next section, the investigations are focused on the deposition of NCD films on AlN-coated ZnO/$LiNbO_3$ substrate, which is the suitable configuration for the WLAW structure.

3.2 NCD deposition on AlN-coated ZnO/$LiNbO_3$ substrates In this part the sample composed of a 300 nm thick AlN layer deposited on a 2 µm thick ZnO film achieved at ambient temperature on $LiNbO_3$ substrate is considered (S3 Sample, Table 1).

The surface morphology of a 300 nm-thick NCD film grown on the AlN-coated ZnO/$LiNbO_3$ substrate is exhibited through the SEM image of Figure 8. A completely homogenous film, showing dense NCD grains, is observed. The surface roughness obtained on the S3 sample, which is about 19 nm, is nearly twice higher than S2 sample (10 nm). It should be noticed that for NCD films thicker than 300 nm, a weak adherence, that may lead to the film delamination, is observed.

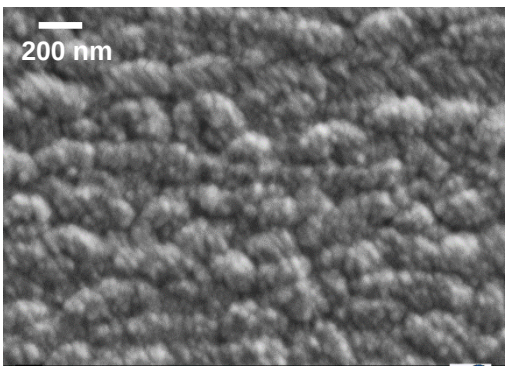

Figure 8 SEM micrograph of NCD film deposited on S3 sample (AlN-coated ZnO/$LiNbO_3$).

The Raman spectra of S3 sample before and after NCD growth presented in Figure 9 are composed of three main component responses. The first range (150-875 cm^{-1}) corresponds mainly to the $LiNbO_3$ contributions [20-23], which intensities are well visible without NCD and significantly decrease after the growth. The Raman peak at 437 cm^{-1} could also be related to the ZnO layer [24], that can be overlapped with $LiNbO_3$ Raman peaks occurring at 426 and/or 448 cm^{-1}. The Raman peak of ZnO at 1150 cm^{-1} is

well defined on AlN-coated ZnO/$LiNbO_3$ substrate but tends to disappear after the NCD growth. Finally, the FWHM of the diamond peak at 1332 cm^{-1} is estimated at 13 cm^{-1}, which is consistent with S2 sample. The principal Raman peak of AlN usually reported at 650 cm^{-1} [25] is not appreciably visible for such a low thickness (300 nm) used for S3 sample.

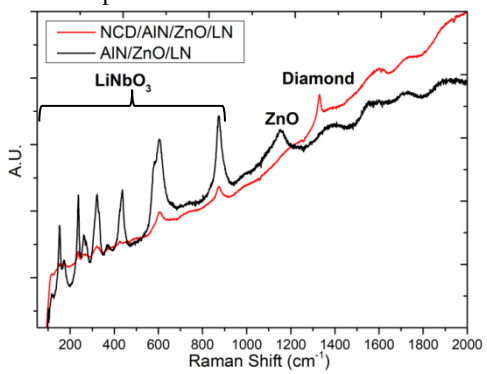

Figure 9 Raman spectra of S3 sample (AlN-coated ZnO/$LiNbO_3$) before and after NCD growth.

The characteristic peaks of AlN (100) and ZnO (103) observed in XRD diffraction patterns of S3 sample after NCD deposition (Figure 10) prove that both materials are still present after the plasma treatment. These peaks are shifted compared to S3 sample before NCD growth. Indeed, AlN(100) diffraction peak appears at 2θ= 36 ° instead of 2θ = 34.6°, and ZnO (103) is at 2θ = 61.8 ° instead of 2θ = 63°. The diamond diffraction peaks ((111) at 2θ=42°, (220) at 2θ=74.7°) observed after deposition are also slightly shifted with respect to S2 sample ((111) at 2θ=43.6°, (220) at 2θ=74.8°).

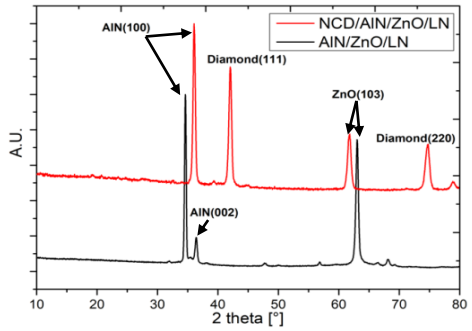

Figure 10 XRD diffraction patterns of S3 sample (AlN-coated ZnO/$LiNbO_3$) before and after NCD growth.

The change of the diffraction peak positions can be mainly attributed to the film strain. For an identical NCD synthesis temperature (250 °C) for S2 and S3 samples, the residual stress is more noteworthy when achieving NCD/AlN/ZnO deposits on $LiNbO_3$ (S3 sample) than on Si (S2 sample). The grain size measured for S3 sample is about 16 nm, which is higher than S1 and S2 samples and leads to the raise of the surface roughness reported before. Nevertheless, S3 sample characterization highlights the successful feasibility of NCD growth on AlN-coated ZnO/$LiNbO_3$ substrate using the DAA system. The ability of the considered NCD deposition process for achieving NCD/AlN/ZnO/IDTs/$LiNbO_3$ WLAW device was then examined.

3.3 NCD deposition on AlN-coated ZnO/IDTs/$LiNbO_3$ substrates for WLAW devices The NCD-based WLAW device achieved on S4 sample is shown in Figure 11. The NCD film covers homogeneously and continuously all the device parts. The adherence of the NCD layer is satisfactory everywhere except on the IDTs finger zone as it is observed in the SEM micrograph of Figure 12 showing the frontier between the IDTs base (on the left) and the IDTs fingers (on the right). Indeed, some cracks are visible on the frontier and the film is bulge on the IDTs finger zone, which in not observed elsewhere. This is due to a lower and inhomogeneous nucleation density resulting from the local topography of the IDTs fingers. Indeed, for such 3D patterns the spin coating method used for nanodiamond particle seeding leads to an inhomogeneous distribution of the nanodiamond particles both on the top and in the space between IDT fingers. Thus, the *ex situ* pretreatment used for enhancing the diamond nucleation must be adapted and optimized for such structure.

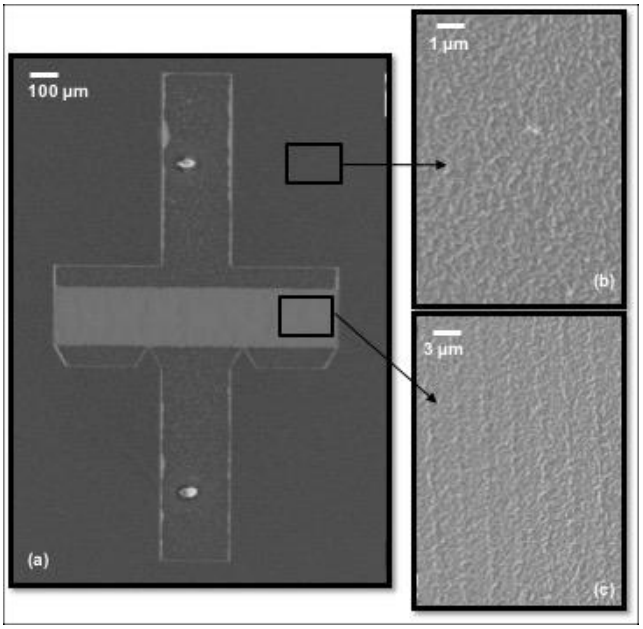

Figure 11 SEM micrograph (back-scattered electrons) of the NCD/AlN/ZnO/IDTs/$LiNbO_3$ WLAW device achieved on S4 sample: (a) global view; (b) focus out of the device; (c) focus of the IDTs finger zone.

The AFM micrograph given in Figure 13 shows the NCD deposited on the IDTs finger zone. In spite of the successive deposition of ZnO, AlN and NCD layers, the shape of the IDTs fingers can be still distinguished. Especially the period λ = 4.4 µm measured from Figure 12 is identical to the value of the initial IDTs/$LiNbO_3$ SAW de-

vice (Figure 1). The width of a single coated finger is now 2 µm instead of 1.32 µm, which shows a filling of the inter-finger volume owing to a conformal growth of the different materials.

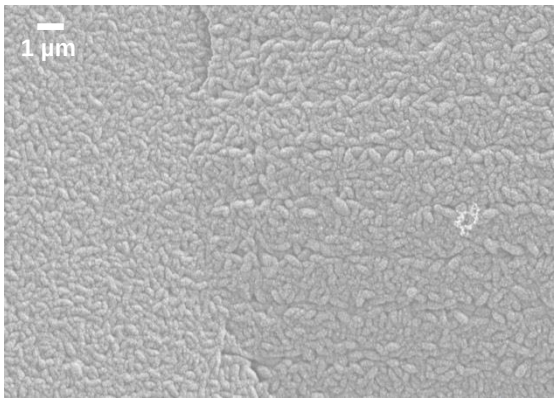

Figure 12 SEM micrograph (secondary electrons) of the IDTs base (on the left) and the IDTs figers (on the right) of the NCD/AlN/ZnO/IDTs/$LiNbO_3$ WLAW device achieved on S4 sample.

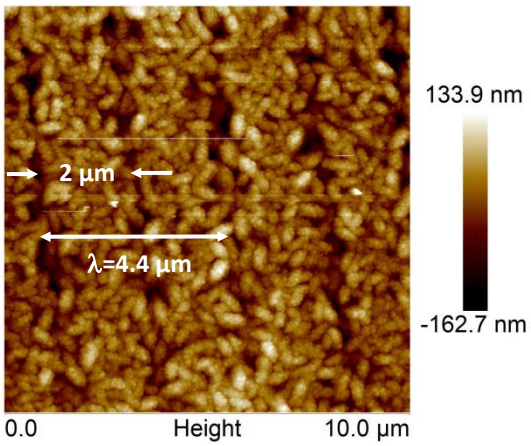

Figure 13 AFM micrograph of the IDTs finger zone of the NCD/AlN/ZnO/IDTs/$LiNbO_3$ WLAW device realized on S4 sample.

Even if some aspects of the NCD synthesis must be further controlled, the feasibility of achieving NCD/AlN/ZnO/IDTs/$LiNbO_3$ layered structure suitable for WLAW device is thus demonstrated.

4 Conclusion In this paper we investigated the NCD deposition on ZnO/Si, ZnO/$LiNbO_3$ and ZnO/IDTs/$LiNbO_3$. The synthesis was carried out in a Distributed Antenna Array microwave system convenient for large area and low temperature deposition, compatible with industrial requirements and temperature sensitive substrates.

The NCD deposition on ZnO substrates necessitates a protective coating in order to prevent the material from plasma etching since a very high etching rate of ZnO is yielded when using $H_2/CH_4/CO_2$ feed gas. The deposition of a thin AlN layer of few hundred nanometers in thickness was shown to be effective to limit the ZnO consumption during the NCD growth process.

First attempts of diamond growth on AlN-coated ZnO/Si substrates pointed out the ability of the DAA reactor to synthesize NCD films with similar properties to those obtained on silicon substrates. The NCD synthesis on AlN-coated ZnO/$LiNbO_3$ substrates showed that the materials involved in the layered structure are stressed. However, adherent NCD films up to 300 nm thickness were synthesized on the considered structure.

Finally, the NCD/AlN/ZnO/IDTs/$LiNbO_3$ layered structure was successfully realized and is promising for WLAW devices. The NCD film adherence is satisfactory, except on the IDTs finger zone.

From the point of view of diamond growth on the AlN-coated ZnO/IDTs/$LiNbO_3$ layered structure, forthcoming works will deal with the improvement of the nucleation enhancement on the IDTs finger zone, and with the reduction of the structure strain during NCD deposition. The characterization of operating NCD-based WLAW devices will also be the subject of future research efforts.

Acknowledgements The authors wish to thank V. Bockelée from LSPM, for technical support and fruitful discussions about NCD film characterization. This work has received support by ANR through projects ANR-11-LABX-086. It was also partially supported by Direction Générale de l'Armement (DGA), the French PIA project "Lorraine Université d'Excellence" (ANR-15-IDEX-04-LUE) and the Institut Carnot en Lorraine (ICEEL).

References

[1] B. Dischler and C. Wild, Low-Pressure Synthetic Diamond: Manufacturing and Applications, Springer Series in Materials Processing, Springer, 1998.
[2] F. Bénédic, M.B. Assouar, F. Mohasseb, O. Elmazria, P. Alnot, and A. Gicquel, Diam. Relat. Mater **13**, 347 (2004).
[3] F. Bénédic, M.B. Assouar, P. Kirsch, D. Monéger, O. Brinza, O. Elmazria, P. Alnot, and A. Gicquel, Diam. Relat. Mater **17**, 804 (2008).
[4] C. Floer, M. Moutaouekkil, F. Bartoli, H. Mishra, S. Hage-Ali, S.M. Murtry, P. Pigeat, O. Elmazria, F. Bartoli, T. Aubert, S. Zhgoon, O. Bou Matar, and A. Talbi, in: 2017 IEEE Int. Ultrason. Symp., 2017: pp. 1–4.
[5] H. Nakahata, K. Higaki, S. Fujii, A. Hachigo, H. Kitabayashi, K. Tanabe, Y. Seki and S. Shikata, in 1995 IEEE Int. Ultrason. Symp. 1995: pp. 361-370.
[6] Y. Fujishima, T. Nishida, M. Shimizu, and T. Shiosaki, in 1993 IEEE Int. Ultrason. Symp. 1993: pp. 263-266.
[7] T. Aubert, O. Elmazria, B. Assouar, E. Blampain, A. Hamdan, D. Genève and S. Weber, IEEE Trans. Ultrason. Ferroelectr. Freq. Control **59**, 999 (2012).
[8] C. Floer, M. Moutaouekkil, F. Bartoli, H. Mishra, S. Mc Murtry, S. Hage-Ali, O. Elmazria, D. Dekkar, B. Baudrillart, F. Bénédic, S. Zhgoon, A. Talbi, O. Bou Matar, F. Bartoli, and T. Aubert, in: IEEE SENSORS, 2017: pp. 1-3.

[9] L. Le Brizoual, O. Elmazria, S. Zhgoon, A. Soussou, F. Sarry, and M. Abdou Djouadi, IEEE Trans. Ultrason. Ferroelectr. Freq. Control **57**, 1 (2010).
[10] B. Baudrillart, F. Bénédic, T. Chauveau, A. Bartholomot, and J. Achard, Diam. Relat. Mater **75,** 44 (2017).
[11] H.A. Mehedi, J. Achard, D. Rats, O. Brinza, A. Tallaire, V. Mille, F. Silva, C. Provent, and A. Gicquel, Diam. Relat. Mater **47**, 58 (2014).
[12] P. Pobedinskas, G. Degutis, W. Dexters, W. Janssen, S.D. Janssens, B. Conings, B. Ruttens, J. D'Haen, H.G. Boyen, A. Hardy, M.K. Van Bael, and K. Haenen, Appl. Phys. Lett **102**, 1 (2013).
[13] H.M. Rietveld, Acta Cryst. **22**, 151 (1967).
[14] B. Baudrillart, F. Bénédic, A.S. Melouani, F.J. Oliveira, R.F. Silva, and J. Achard, Phys. Status Solidi A **213,** 2575 (2016).
[15] B. Baudrillart, F. Bénédic, A. Tardieu, and J. Achard, Phys. Status Solidi A **214**, 1700205 (2017).
[16] B. Baudrillart, F. Bénédic, O. Brinza, T. Bieber, T. Chauveau, J. Achard, and A. Gicquel, Phys. Status Solidi A **212**, 2611 (2015).
[17] I. Calizo, K.A. Alim, V.A. Fonoberov, S.Krishnakumar, M. Shamsa, A.A. Balandinand, and R. Kurtz, Proc. SPIE 6481, Quantum Dots, Particles, and Nanoclusters IV, **64810N** (2007).
[18] A.C. Ferrari and J. Robertson, Phys. Rev. B **63**, 121405 (2001).
[19] A. Taabouche, A. Bouabellou, F. Kermiche, F. Hanini, S. Menakh, Y. Bouachiba, T. Kerdja, C. Benazzouz, M. Bouafia, and S. Amara, Adv. Mater. Phys. Chem **03**, 209 (2013).
[20] F. Jermann, S. Klauer, U. Schlarb, and M. Wohlecke, Appl. Phys. A, **56**, 103 (1993).
[21] A. Ridah, P. Bourson, M. D. Fontana, and G. Malovichko, J. Phys. Condens. Matter. **9**, 9687 (1997).
[22] Y. Repelin, E. Husson, F. Bennani, and C. Proust, J. Phys. Chem. Solids **60**, 819 (1999).
[23] V. Caciuc, A. V. Postnikov, and G. Borstel, Phys. Rev **61**, 8806 (2000).
[24] C. V. Hernandez, F.N. Jiménez-García, J.F. Jurado, and V.H. Granada, Microelectron. J. **39**, 1347 (2008).
[25] I.C. Oliveira, C. Otani, H.S. Maciel, M. Mass, L.K. Noda, and M.L.A. Temperini, J. Mater. Sci. Mater. Electron. **12**, 259 (2001).